Observation of nonspherical particle behaviors for continuous shape-based separation using hydrodynamic filtration

Sari Sugaya, Masumi Yamada, and Minoru Seki[a)]
Department of Applied Chemistry and Biotechnology, Graduate School of Engineering, Chiba University, 1-33 Yayoi-cho, Inage-ku, Chiba 263-8522, Japan

(Received 20 January 2011; accepted 29 March 2011; published online 20 April 2011)

Selection of particles or cells of specific shapes from a complex mixture is an essential procedure for various biological and industrial applications, including synchronization of the cell cycle, classification of environmental bacteria, and elimination of aggregates from synthesized particles. Here, we investigate the separation behaviors of nonspherical and spherical particles/cells in the hydrodynamic filtration (HDF) scheme, which was previously developed for continuous size-dependent particle/cell separation. Nonspherical particle models were prepared by coating the hemisphere of spherical polymer particles with a thin Au layer and by bonding the Janus particles to form twins and triplets resembling dividing and aggregating cells, respectively. High-speed imaging revealed a difference in the separation behaviors of spherical and nonspherical particles at a branch point; nonspherical particles showed rotation behavior and did not enter the branch channel even when their minor axis was smaller than the virtual width of the flow region entering the branch channel, w_1. The confocal-laser high-speed particle intensity velocimetry system visualized the flow profile inside the HDF microchannel, demonstrating that the steep flow-velocity distribution at the branch point is the main factor causing the rotation behavior of nonspherical particles. As applications, we successfully separated spherical and nonspherical particles with various major/minor lengths and also demonstrated the selection of budding/single cells from a yeast cell mixture. We therefore conclude that the HDF scheme can be used for continuous shape-based particle/cell separation. © *2011 American Institute of Physics.* [doi:10.1063/1.3580757]

I. INTRODUCTION

Shape is one of the most important factors characterizing cell species, types, and cell states. For example, prokaryotes are classified into four basic groups (cocci, bacilli, vibrio, and spirochaete) mainly based on shape.[1,2] Also, eukaryotic cells show cell-cycle dependent physical changes in shape;[3,4] for example, budding yeast cells (*Saccharomyces cerevisiae*) change their shapes during proliferation from a sphere to a bispherical twin or a larger aggregate, depending on their cell-cycle stages.[4] In addition, the mammalian cancerous lymphocytes show the morphological transformation from a sphere into a ellipsoid or even a bispherical twin with the passage of the cell-cycle stages from G2 phase to M phase.[5] A technique for shape-based cell separation would therefore be essential for the synchronization of cell cycles, classification of environmental bacteria, and even the elimination of aggregates from synthesized particles. Various types of conventional techniques are available to separate cells based on the physical/chemical properties of cells, from simple centrifugation and filtration techniques to the highly sophisticated FACS devices.

[a)]Electronic mail: mseki@faculty.chiba-u.jp. Tel./FAX: +81-43-290-3436.

However, these techniques are not able to achieve purely shape-based cell separation since most of them utilize the cell size, density, or surface properties for separation instead of the cell shape.

Recently, microfluidic technologies have been utilized as a means to precisely separate small samples such as cells, particles, and biomacromolecules.[6,7] As the continuous separation methods of cells/particles in microfluidic devices, researchers have combined the stable laminar flow and the external physical forces such as dielectrophoretic,[8–12] acoustic,[13,14] gravitational,[15] magnetic,[16,17] and optical[18] forces. Separation techniques solely utilizing the microscale hydrodynamics have also been reported, e.g., pinched-flow fractionation,[19,20] hydrodynamic filtration and similar techniques,[21–26] deterministic lateral displacement,[27,28] inertial-flow focusing,[29–31] Dean flow-based separation,[32,33] hydrophoresis,[34,35] deformability-based cell margination,[36] and so on, achieving passive and continuous separation of cells/particles based on size, density, or deformability, without necessitating external forces or labeling techniques. Although these methods enable the efficient and precise separation of particulate samples from bacterial cells to large animal cells, most of the separation mechanisms are based on the assumption that the target objects are spherical, and there has been no discussion of the separation behavior of nonspherical objects having complicated morphologies.

Erythrocytes are the only exception; erythrocytes are disk-shaped and their behavior in microchannels has been studied. Tegenfeldt and co-workers[37,38] reported a difference in the separation behaviors of erythrocytes in the lateral displacement microchannels depending on the height of the micropillars. When the micropillar height is sufficiently small, erythrocytes are separated based on the largest diameter (i.e., the disk diameter), while the disk thickness of erythrocytes is recognized in the case of higher micropillars. These results demonstrate the applicability of microfluidic schemes for shape-based separation, but this concept cannot be directly employed to explain the behaviors of general nonspherical particles, first because erythrocytes are highly unique in terms of shape, size, and deformability, and second there have not been appropriate models available for the other types of nonspherical particles. A technique for achieving shape-based particle/cell separation would become an essential procedure for industrial/research applications; for example, shape-based cell-cycle synchronization would be possible without employing specific chemical treatments, which are usually conducted in biological experiments.[4,39]

In the present study, we examined the applicability of the hydrodynamic filtration (HDF) technique for the shape-based separation of nonspherical particles; this technique was previously developed for size-based sorting of particles/cells (typically with a diameter of $1-100\ \mu$m) using a microchannel network composed of a main channel and a number of branch channels. We have demonstrated the separations of blood cells and liver cells using the HDF technique, proving its potential for actual biomedical applications.[22,24] However, the particle/cell shapes were assumed to be spherical, and the behaviors of the particles having different shortest and longest diameters have not been discussed; even the erythrocytes were regarded as spheres with a diameter of $\sim 3\ \mu$m. Figure 1(a) shows the basic principle of separation behaviors of spherical particles at a branch point. A thin region of the fluid flowing near the lower sidewall (with a width of w_1) is split into the branch channel. If the center position of a particle is outside this region, it never flows into the branch channel. On the other hand, small particles with the center positions in this region are removed from the main stream through the branch channel. The width of this virtual flow region, w_1, is determined by the width of the main channel and the distribution ratio of flow rates into the branch channel; the distribution ratio is freely controlled by precisely designing the microchannel network regarding as a resistive circuit. Because of the presence of the parabolic flow-velocity distribution, it is naturally anticipated that the spherical particles are rotating, as shown in Fig. 1(b), when they are flowing near the sidewall. In the case of rodlike, disklike, or bispherical particles flowing in a laminar flow system, the major axes (the largest diameters) of such particles would be in parallel to the flow direction. Figures 1(c) and 1(d) show the possible behaviors of nonspherical twin particles at a branch point. If such nonspherical particles show rotation behaviors in the vicinity of the channel wall and the branch point, as shown in Fig. 1(c), a difference would arise in the separation behaviors of the spherical and nonspherical particles, although the shortest diameters of these particles are the same [Fig. 1(c)]. When the center position of the

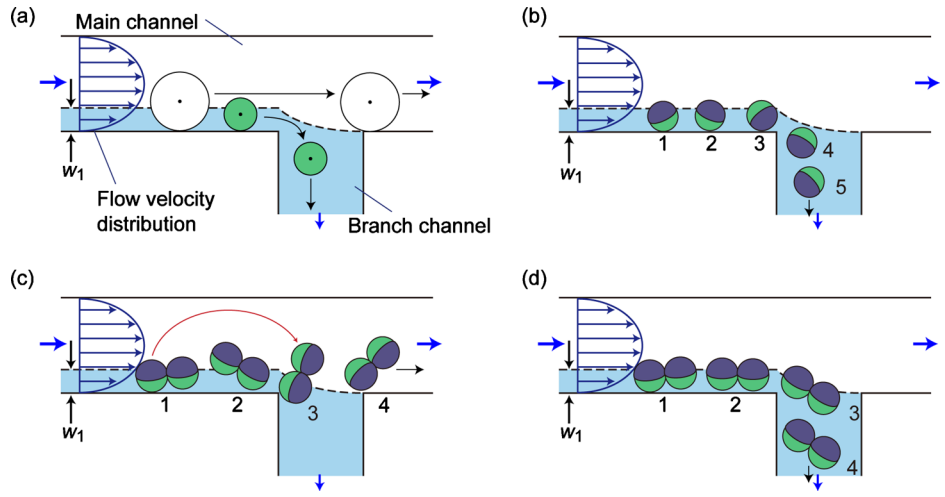

FIG. 1. Schematic diagrams showing the separation behaviors of particles in the HDF scheme. (a) Size-dependent separation of spherical particles and [(b)–(d)] possible rotation behaviors of spherical (b) and nonspherical [(c) and (d)] particles at the branch point.

nonspherical particles crosses the boundary between the flow regions (shown by the dotted line in the figure) due to the rotation, such particles would not flow into the branch channel. In contrast, if nonspherical particles do not rotate, the center position would be the same as that of the spherical particles, making separation impossible [Fig. 1(d)].

In order to prepare a nonspherical particle model, we propose a fabrication method for twin or triplet particles from spherical polymer particles having Janus morphology, which are suitable for observing the rotation movement. To visualize the particle movement, a high-speed imaging system was used, and the flow profile was observed by using a high-speed microparticle intensity velocimetry (micro-PIV) system. In addition, we demonstrate the separation of spherical/nonspherical particles and the sorting of budding yeast cells according to their morphologies.

II. EXPERIMENTAL SECTION

A. Materials

Green fluorescent polystyrene microbeads, 1.0 or 10 μm in diameter, and nonfluorescent polymer microbeads, 15 or 20 μm in diameter, were obtained from Duke Scientific Corp., CA, USA. Fluorescent particles with a diameter of 0.5 μm (F8813) were obtained from Invitrogen Corp., CA, USA. Ethanol (99.5%), sucrose, glucose, Tween 80, and adenine sulfate were purchased from Wako Purechemical Ind., Ltd., Japan. For microdevice fabrication, negative photoresists, SU-8 3015, and 3025 (MicroChem Corp., MA, USA), and PDMS (polydimethylsiloxane; Silpot 184 W/C; Dow Corning Toray Co., Ltd., Japan) were used. Bacto pepton and yeast extract were purchased from Becton, Dickinson and Co., NJ, USA.

B. Fabrication of nonspherical particles

The fabrication procedures of nonspherical Janus particles are shown in Fig. 2(a). First, spherical Janus particles were prepared by following the previously reported procedure.[40] A suspension of fluorescent particles (10 μm in diameter) in ethanol was dropped on a glass slide and dried, forming a monolayer of particles. The surface was then treated by oxygen plasma at 100 W for 30 s using a plasma reactor (PR500, Yamato Scientific Co., Ltd., Japan), following the coating of the upper hemispheres of the particles with a thin layer of Au (thickness of $\sim$20 nm) using a magnetron sputtering system (MSP-1S, Vacuum Device Inc., Japan). The half-coated Janus particles were recovered from the glass slide and suspended in ethanol by sonication. A centrifugation process was then employed to bond the Janus particles by utilizing the plasticity of the Au layer.

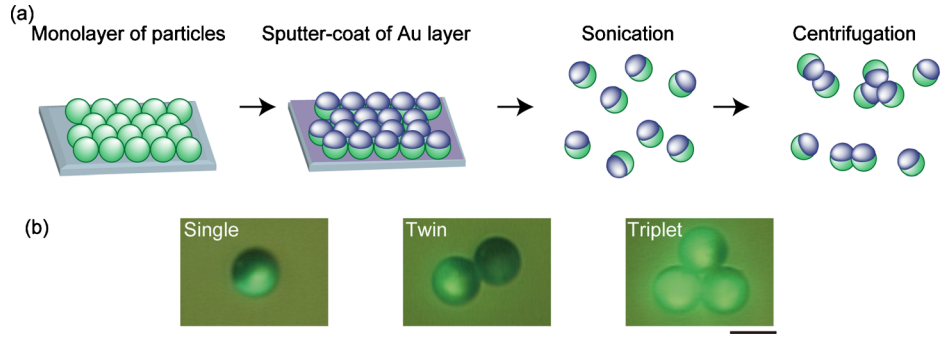

FIG. 2. (a) Fabrication process of nonspherical particle models. Janus particles are initially prepared and then bonded to form nonspherical twin and triplet particles. (b) Micrographs of the fabricated single, twin, and triplet particles. Scale bar: 10 μm.

The particle suspension in ethanol was centrifuged at 2000 G for 30 s using a centrifuge device (Himac CT13R, Hitachi Ltd., Japan). Centrifuged particles were resuspended by vortexing, and the centrifugation process was repeated five times to increase the presence of twins/triples [Fig. 2(b)]. To remove the Au debris and the aggregated particles composed of more than four single particles, particles were filtered through a nylon mesh with 20 μm pores (PP-20N, Kyoshin Rikoh Inc., Japan).

C. Microdevice fabrication and design

Microdevices were fabricated by using soft lithography and replica molding techniques, as described previously.[41,42] Initially, SU-8 structures were patterned on Si wafers to prepare molds, and the PDMS replica was then obtained. The PDMS plate having channel structures was bonded with a flat glass slide after O_2 plasma treatment.

Two types of microdevices were employed in this study: microdevices A and B. Microdevice A was designed for the separation of particles with diameters ranging from 10 to 20 μm and used for the observation of behaviors of fabricated nonspherical particles [Fig. 3(a)]. This device was equipped with two inlets and six outlets. Inlets 1 and 2 were used for introducing fluid flows with and without containing particles, respectively; the fluid flow from inlet 2 allowed the perfect focusing of particles/cells to the lower sidewall after passing through the 65 branch points connected to outlet 6. The main channel width was 90 μm and was connected to 130 branch channels; 20, 15, 15, 15, and 65 branch channels were connected to outlets 2, 3, 4, 5, and 6, respectively. Each branch channel was composed of narrow (30 μm) and wide (40 or 45 μm) segments

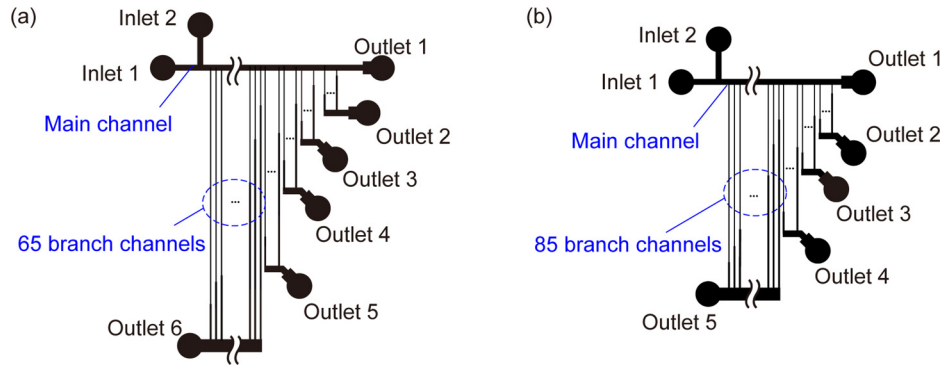

FIG. 3. Schematic illustrations of the designs of HDF microchannels. (a) Microdevice A for particle separation and (b) microdevice B for sorting budding yeast cells. Details of these microchannels are shown in the supplemental information (Ref. 43). Drawing is not to scale.

TABLE I. The measured and theoretical values of the virtual width of the flow region entering the branch channels connected to each outlet (w_1). The unit is μm.

	Outlet 2	Outlet 3	Outlet 4	Outlet 5	Outlet 6
Measured	9.0	8.6	7.6	7.0	5.7
Theoretical	10.0	9.0	8.0	7.0	6.0

to properly adjust the hydrodynamic resistance while keeping the lengths of branch channels uniform. The channel depth was uniform, 26 μm. The theoretical values of the virtual widths of the flow region entering the branch channels, w_1, are shown in Table I. It was expected that particles with sizes >20, 18–20, 16–18, 14–16, 12–14, and <12 μm would be recovered from outlets 1, 2, 3, 4, 5, and 6, respectively.

Microdevice B was designed for the separation of budding yeast cells [Fig. 3(b)]. This device had two inlets and five outlets, with a main channel width of 30 μm, which was connected to 113 branch channels; 8, 8, 12, and 85 branch channels were connected to outlets 2, 3, 4, and 5, respectively. Each branch channel was composed of narrow (10 μm) and wide (20 or 30 μm) segments. The channel depth was 12 μm. The detailed structures of microdevices A and B are shown in the supplemental information.[43]

D. Microfluidic experiments

First, to investigate whether the fabricated devices worked as we designed, the volumetric flow rate distributed to each outlet was measured by introducing distilled water from inlets 1 and 2 using syringe pumps (KDS200, KD Scientific Ink., MA, USA) and measuring the output volumes. Also, to measure the virtual widths of the flow regions entering the branch channels, w_1, fluorescent microparticles were introduced and their movements were observed by using an ICCD (Intensified CCD) camera (C2400-89V, Hamamatsu Photonics K.K., Japan) through an inverted fluorescence microscope (IX70, Olympus Corp., Japan). To observe the behaviors of spherical and nonspherical particles in microdevice A, single, twin, and triplet Janus particles were suspended in distilled water containing 15% (w/w) sucrose and 0.5% (v/v) Tween 80 at a total concentration of 1×10^6 particles/ml. Aqueous solutions with and without containing particles were introduced from inlets 1 and 2 at 3 μl/min, respectively. Particle behaviors were video-captured at 1000 flames/s using a high-speed camera (VCC-H1000C, DigiMo Co., Ltd., Japan). In addition, the flow profile was visualized by employing a high-speed micro-PIV system (confocal scanning micro-PIV system, Seika Corp., Japan). Fluorescent particles ($\oslash$=0.5 μm) were suspended in 0.5% (v/v) Tween 80 aqueous solution and introduced into microdevice A, and images of particle movement were captured at 2000 flames/s. The flow-velocity distribution was calculated and visualized using an image analyzing software (KONCERT, Seika Corp., Japan). To demonstrate the shape-based particle separation, spherical and nonspherical particles were mixed and introduced into microdevice A, and the separation behaviors were observed. The fabricated nonspherical twin/triplet particles and the spherical particles, 10, 15, and 20 μm in diameter, were suspended in the same aqueous solution as described above. The solutions with and without containing particles were introduced from inlets 1 and 2 of microdevice A at 30 μl/min by using syringe pumps, respectively. The separated particles were recovered from each outlet, and their numbers and concentrations were measured.

E. Sorting of budding yeast cells

Saccharomyces cerevisiae (BY 23849) was cultured in YPDA (yeast peptone dextrose adenine) medium, composed of 2% bacto pepton, 1% yeast extract, 2% glucose, and 1% adenine sulfate at 27 °C for 24 h and resuspended in the medium at 1×10^8 cells/ml. The yeast suspension and the medium were introduced from inlets 1 and 2 of microdevice B at 15 μl/min,

TABLE II. Comparison of the measured and theoretical values of volumetric flow rates distributed into each outlet of microdevice A. The unit is % of the total introduced volumetric flow rate.

	Outlet 1	Outlet 2	Outlet 3	Outlet 4	Outlet 5	Outlet 6
Measured	6.93	8.06	7.68	9.11	13.46	54.55
Theoretical	7.76	7.84	8.28	9.61	9.96	56.55

respectively. Sorted cells were recovered from each outlet and then immediately placed on ice to prevent cell growth, and their morphologies were observed.

III. RESULTS AND DISCUSSION

A. Fabrication of nonspherical particles

Although researchers have proposed methods to prepare nonspherical particles, including *in situ* photopolymerization in microfluidic devices,[44–46] seeding polymerization,[47] and droplet coalescence,[48] we proposed a procedure to easily fabricate nonspherical particles from spherical Janus particles, which is suitable to observe the rotation movement in the HDF microchannels. Initially, the hemispheres of the fluorescent polymer particles were covered with opaque Au layers and the fluorescence was partially disappeared. Then, by applying centrifugation processes, Janus particles were bonded together via the Au surface to form twins or triplets [Fig. 2(b)]. After the first centrifugation process, the ratios of single, twin, and triplet particles were 86.7%, 11.5%, and 1.8%, respectively. The ratios of twins and triplets were increased by repeating the centrifugation processes after resuspending the particles by vortexing; the ratios of singles, twins, and triplets were 67.6%, 19.8%, and 12.6%, respectively, after five centrifugation cycles. This increase was due to the enhanced possibility of collisions between the particles since the bonding occurred by the contingence of Au surfaces on the hemispheres of particles when they were in contact in the direction of the centrifugal force. Note that the presence of particle aggregates composed of more than four singles was increased when the centrifugation processes were repeated, but that these large aggregates were removed by filtration. In the following experiments, we used the particle mixture prepared by the five-cycle centrifugation processes. The bonding of these particles was highly stable; bonded particles were not torn apart into single particles even by vortexing or by introducing into the microchannels.

B. Evaluation of microdevices

Before conducting particle separation, we examined whether the two types of microchannels were properly fabricated as we designed. First, the volumetric flow rates distributed to each outlet were measured. The theoretical and experimental results are shown in Tables II and III; these values showed good agreements for microdevices A and B, although these microfluidic networks were composed of more than 100 branch channels. The slight differences between the theoretical and experimental were likely due to the partial nonuniformity in the depth of the microchannels.

The virtual widths of the flow region (w_1) entering the branch channels were evaluated for microdevice A by tracking the movements of florescent particles with a diameter of 1.0 μm. The flow rates of the particle suspension from inlets 1 and 2 were the same, 0.5 μl/min. Figure 4

TABLE III. Comparison of the measured and theoretical values of volumetric flow rates distributed into each outlet of microdevice B. The unit is % of the total introduced volumetric flow rate.

	Outlet 1	Outlet 2	Outlet 3	Outlet 4	Outlet 5
Measured	9.46	10.54	10.74	14.45	54.80
Theoretical	11.05	10.72	10.67	10.81	56.75

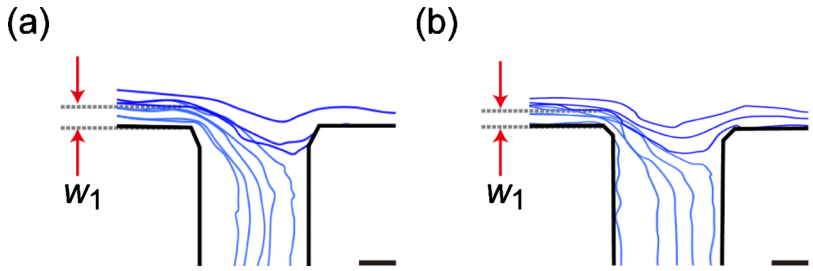

FIG. 4. Visualization of the virtual regions entering into branch channels connected to (a) outlet 2 and (b) outlet 6. The widths of the flow region entering the branch channels, w_1, were (a) 9.0 and (b) 5.7 μm, respectively. Scale bar: 10 μm.

shows the tracks of particle movement at branch points connected to outlets 2 (a) and 6 (b), respectively. We defined the value of w_1 as the distance from the lower sidewall to the boundary of the flow regions, as indicated by the two arrows in the figure. The comparisons of the theoretical and measured values of w_1 for outlets 2–6 are shown in Table I. Although the experimental values of w_1 were slightly smaller than the theoretical values, the values generally showed a good correspondence. From these results, it was expected that spherical particles with diameters of $>$18.0, 17.2–18.0, 15.1–17.2, 14.1–15.1, 11.4–14.1, and $<$11.4 μm would be recovered from outlets 1, 2, 3, 4, 5, and 6, respectively.

C. Separation behaviors of nonspherical particles

To exploit the potential of the HDF scheme for the shape-based particle/cell separation, the behaviors of spherical and nonspherical particle were visualized using a high-speed video camera system. Figure 5 and videos show the behaviors of single and twin particles at the branch point to outlet 6 of microdevice A when the each flow rate from inlets 1 and 2 was 3 μl/min. The single and twin particles were rotating at the vicinity of the sidewall, and thus, there was a difference in the average distances from the center position of these particles to the lower sidewall; the distances were 5 and 6.3 μm for singles and twins, respectively. Also, almost all of the twin particles showed a 180° rotation at the branch point, and this rotation moved the center position of twin particles out of the flow region entering the branch channel, which caused the different separation behavior from that of the single particles. As a result, twin particles did not flow to outlet 6 (w_1 =5.7 μm) but flowed to outlet 5 (w_1=7.0 μm). These results showed that particles with the same shortest diameter but different largest diameters could accurately be separated, demonstrating the possibility for shape-based separation in the HDF scheme. The rotation behavior of the nonspherical triplet particle was also observed, as shown in the supplemental information.[43]

The parabolic flow-velocity profile in laminar flow systems is the most probable factor that caused the rotation behavior of the twin particles, and thus, we visualized the flow profile by using the high-speed confocal PIV system. The visualized profile in the z=13 μm plane of the 26 μm deep microchannel, using 0.5 μm particles as tracers with the total inlet flow rate of 0.3 μl/min, is shown in Fig. 6(a). The flow velocity at the center of the main channel was faster ($\sim$1300 μm/s) than that in the vicinity of the sidewall or in the branch channel. In order to clarify the different flow forces applied to the two particles comprising a twin, we defined the x- and y-axes, as shown in Fig. 6(b), and analyzed the flow-velocity distributions along the x=1.9 μm line; the major axis of the twin particle at 4 ms in Fig. 5(b) was almost parallel to the y-axis on this line. In this micrograph, the center positions of particles (a) and (b) were (x, y=1.9, 11.4) and (x, y=1.9, 1.9), respectively. Figures 6(c) and 6(d) show the flow velocities in the x (v_x) and y (v_y) directions on the x=1.9 μm line, respectively; v_x for the center positions of particles (a) and (b) were 561 and 104 μm/s, respectively, and v_y were $-$263 and $-$125 μm/s, respectively. Figure 6(e) shows the particle positions and the flow vectors at the center positions of the twin particle at 4 and 8 ms in Fig. 5(b). At the entrance of the branch point [at 4 ms in Fig. 5(b)], the flow force applied to particle (a) is greater than that to particle (b), which generated the

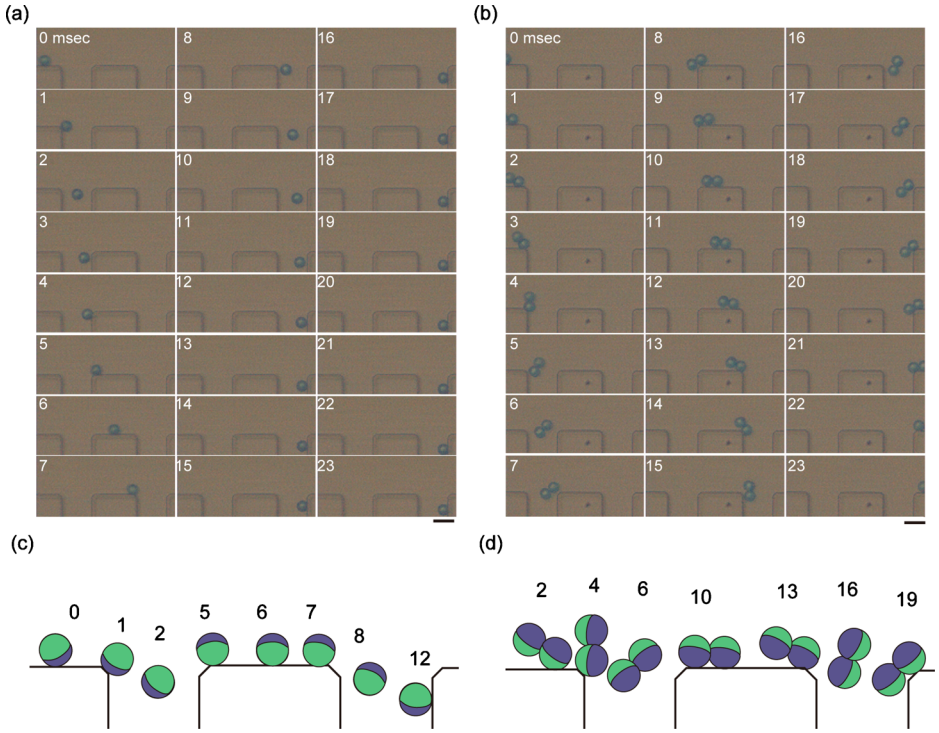

FIG. 5. Behaviors of single and twin particles at a branch point connected to outlet 6 in microdevice A. [(a) and (b)] Micrographs of (a) a spherical particle and (b) a nonspherical twin particle at every 1 ms. Scale bar: 20 μm. [(c) and (d)] Schematic illustrations of positions of (c) spherical and (d) nonspherical twin particle micrographs. The numbers correspond to the times (ms) shown in (a) and (b) (enhanced online). [URL: http://dx.doi.org/10.1063/1.3580757.1] [URL: http://dx.doi.org/10.1063/1.3580757.2]

moment to rotate the twin particles. At 8 ms, v_x for the center positions of particles (a) and (b) were 276 and 90.9 μm/s, respectively, and v_y were 93.5 and 28.1 μm/s, respectively, indicating that the twin particle goes upward and does not flow into the branch channel. We confirmed that the twin particles showed 180° rotation at the branch point without exception.

D. Separation of particles with various largest/shortest diameters

Although we separated particles with the same shortest diameter but different longest diameters as described in Sec. III C, it is also necessary to demonstrate the separation of particles with various longest/shortest diameters for general shape-based particle separation. We therefore tried to separate the mixture of particles, as shown in Fig. 7(a); spherical ($\oslash$=10, 15, and 20 μm) and nonspherical (twin and triplet) particles were mixed and introduced into microdevice A, and their separation behaviors were examined. The particles recovered from each outlet were counted for each type of particle. Figure 7(b) shows the micrographs of the recovered particles, and Fig. 7(c) shows the ratio of each particle. The nonspherical twin particles, with shortest and longest diameters of 10 and 20 μm, respectively, were separated from the three types of spherical particles ($\oslash$=10, 15, and 20 μm), and were mainly recovered from outlet 5; the ratio of twin particles recovered from outlet 5 was 81.1%. This result suggests that the separation mechanism of nonspherical particles in the HDF scheme is based both on the shortest and longest diameters of particles, proving the ability of the HDF scheme to carry out shape-based particle separation.

In the case of the triplet particles, they were recovered from outlets 1–5. This wide distribution was due to the existence of various types of triplet particles, as shown in Fig. 7(a). The shortest diameter of the triplet particle is the same as that of single particles, regardless of the binding angles. On the other hand, the longest diameters varied from 20 to 30 μm, depending on the

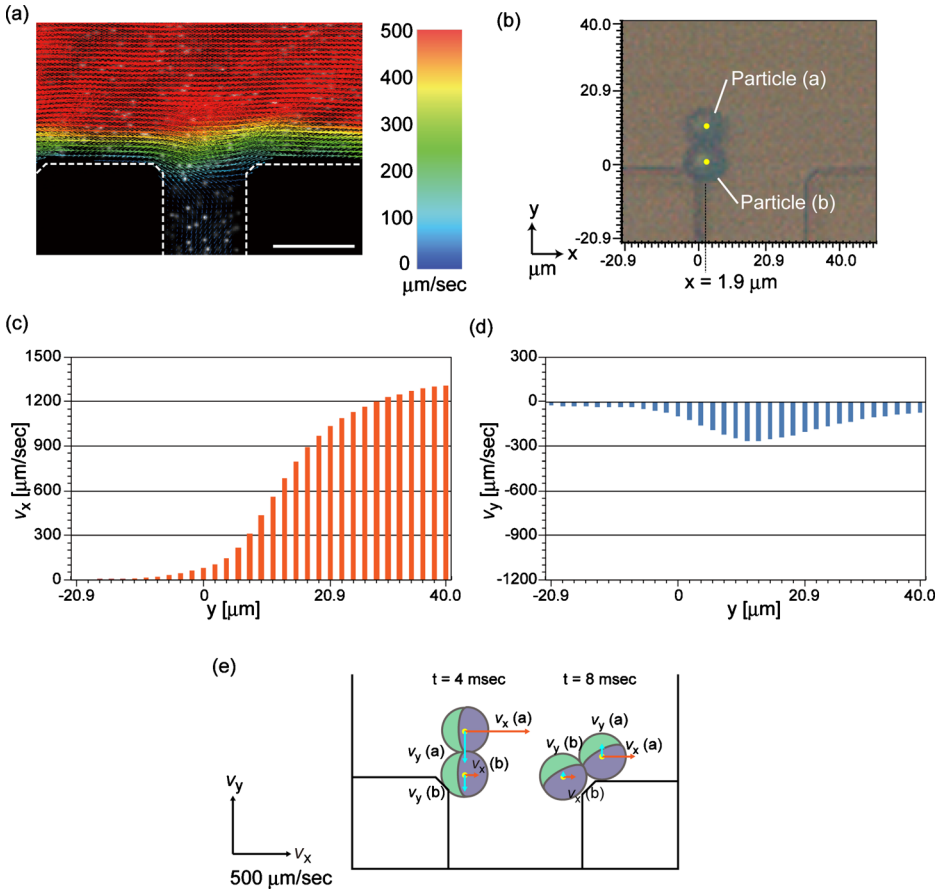

FIG. 6. Visualized flow-velocity distribution at a branch point connected to outlet 6 in microdevice A when the inlet flow rate was 2.0 μl/min. (a) Image showing the flow-velocity distribution. Scale bar: 30 μm. (b) Definition of x- and y-axes at the branch point. The location of a nonspherical twin particle corresponds to that shown in Fig. 5(a) at 4 ms. [(c) and (d)] The distributions of flow velocities (c) v_x and (d) v_y along the x=1.91 μm line. (e) Schematic image showing the flow forces in the x- and y-directions on the twin particle. The particle positions correspond to those at 4 and 8 ms in Fig. 5(b).

binding angle, and this variation caused the different rotating motions at the branch point. Almost all of the triplet particles collected from outlet 4 showed an equilateral trianglelike shape, having the same longest and shortest diameters as those of twins; this result also demonstrated shape-based separation for particles with the same longest and shortest lengths but different volumes.

Although most of the twin particles were recovered from outlet 5, some were separated from outlets 4 and 6; 12.1% and 3.5% of the introduced twin particles were recovered from outlets 4 and 6, respectively. This imperfection in the separation accuracy might have been caused by the disordered behaviors of particle rotation at the branch points. That is, when particles were flowing in the microchannel and the rotating axis was not parallel to the depth direction of the main channel, these twin particles behaved like single particles and were recovered upstream from outlet 6, even though the frequency of these particles was not as high. On the other hand, we observed irregularly rotating particles apart from the sidewall that did not enter the branch channels to outlet 5 but flowed into downstream branches connected to outlet 4. The decrease in the microchannel depth (desirably less than the largest diameter of the nonspherical particles) would prevent the irregular rotation of particles with a rotation axis not parallel to the depth direction and improve the separation accuracy.

E. Sorting of budding yeast cells

To examine the applicability of the presented shape-based separation scheme to biological samples, budding yeast cells [*Saccharomyces cerevisiae* (BY 23849)] were sorted. Yeast cells

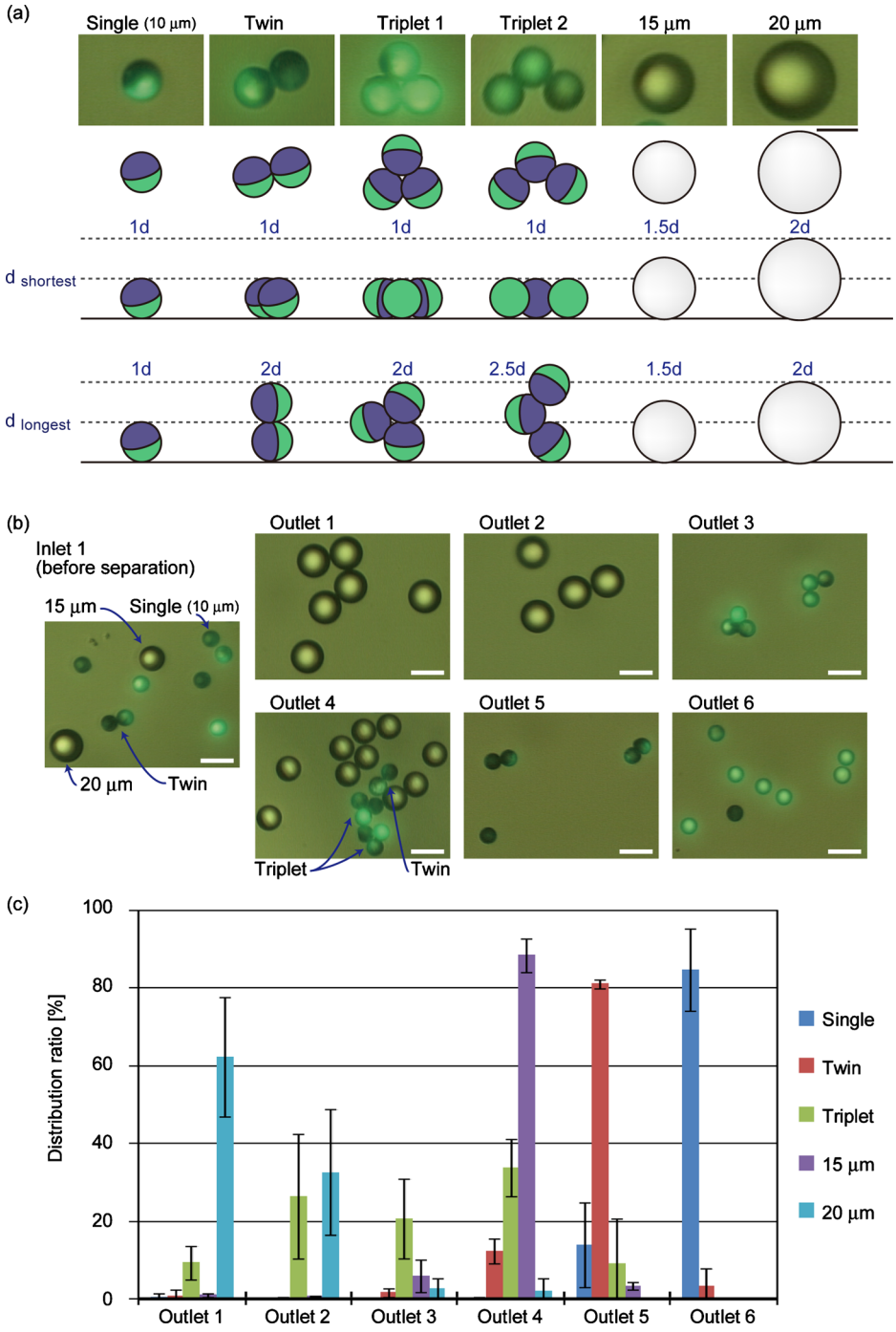

FIG. 7. Separation results for spherical and nonspherical particles. (a) Micrographs and schematic diagrams of spherical and nonspherical particles used for separation. Scale bar: 10 μm. The sizes of the triplets varied depending on the bonding angles, which were 60° and 110° for triplets 1 and 2. (b) Micrographs of particles before separation and after recovery from outlets 1–6. Scale bar: 20 μm. (c) Distribution ratios of particles at each outlet. Each value shows the mean ± SD from three independent experiments.

show various morphologies depending on the cell states[4,49–51] and are categorized into single, budding twin, and aggregates composed of more than three cells, and the diameters are typically in the range of 3–10 μm. Cells were suspended in the medium and introduced into microdevice B.

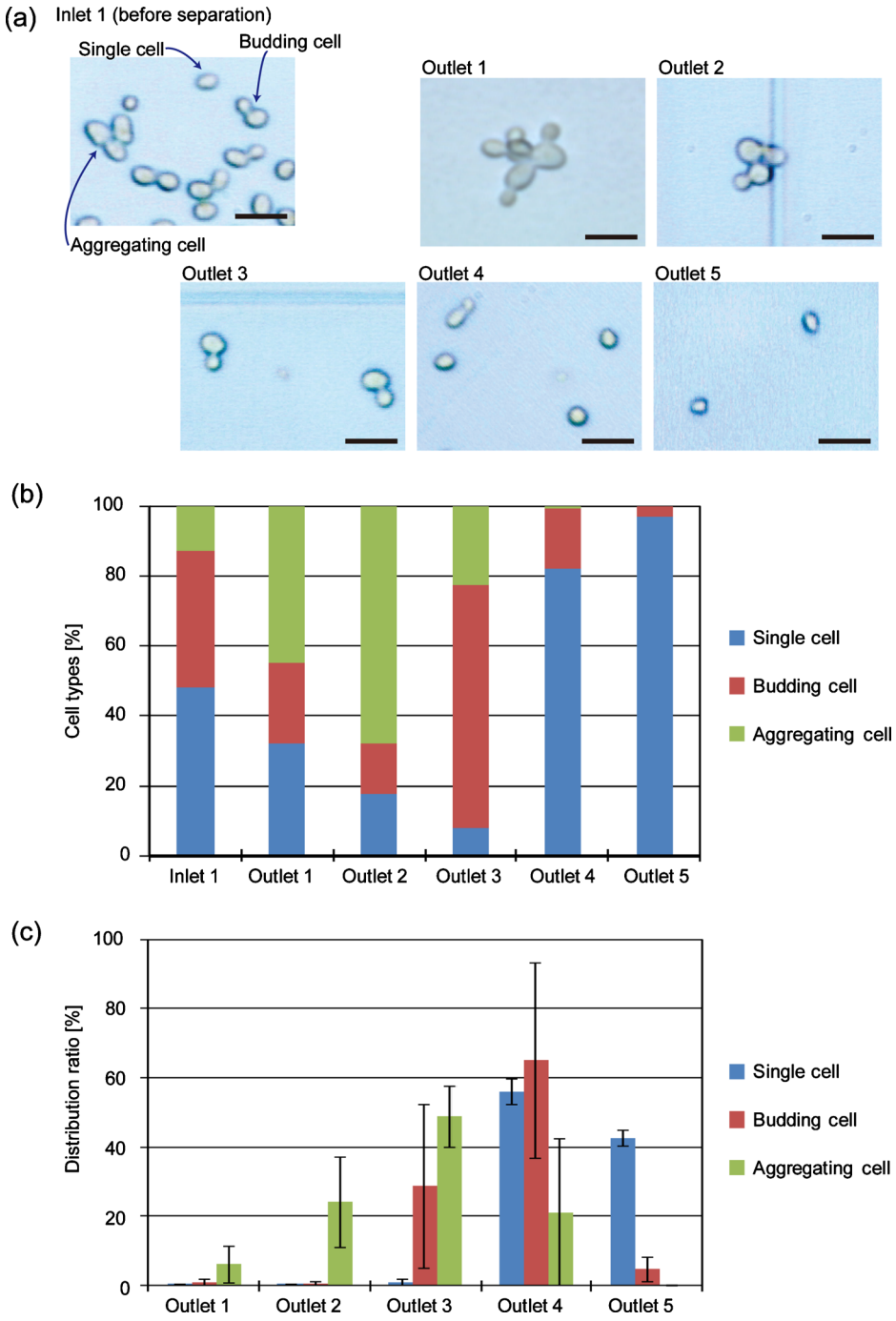

FIG. 8. Sorting results for budding yeast cells. (a) Micrographs of cells before separation and after recovery from outlets 1–5. Scale bar: 10 μm. (b) The ratios of cell types in the fractions recovered from each outlet and (c) the distribution ratios of cells according to cell type. Each value shows the mean ± SD from three independent experiments.

The results of the budding yeast separation are shown in Fig. 8. Before separation, the ratios of single, budding, and aggregated cells were 48.0%, 39.4%, and 12.6%, respectively. After separation using the microdevice, most of the single cells were recovered from outlets 4 (56.2%) and 5 (42.6%), while budding cells composed of mother and daughter cells were mainly recovered from outlets 3 (28.8%) and 4 (65.2%). The populations of aggregated cells were significantly low

in the fractions recovered from outlets 4 and 5. The ratios of single cells in the fractions from outlets 4 and 5 were high, 82.1% and 97.0%, respectively, while that of the budding twin cells in the fraction from outlet 3 was 69.4%, demonstrating the relatively high separation efficiency of budding yeast cells depending on the cell morphologies. These results demonstrated the ability of the HDF scheme to perform cell-cycle synchronization not only by utilizing the size difference but also by employing the difference in cell morphologies, without using specific chemicals such as thymidine, nocodazole, or colcemid, temperature-sensitive cell-cycle (cdc) mutants.[4,39]

IV. CONCLUSIONS

We have successfully shown the applicability of the HDF scheme for particle/cell sorting based on shape. First, we developed a fabrication process for nonspherical particles utilizing the Janus particles and the plasticity of the Au surface. The prepared nonspherical twin/triplet particles were used for the observation of separation behaviors. The different rotation behaviors of spherical and nonspherical particles were visualized and found to be caused by the flow-velocity distribution at the branch point. Shape-based particle separation was then achieved, and the sorting of budding yeast cells was demonstrated based on their morphologies. The presented separation scheme utilizing the different rotation behaviors of different particle types would be a valuable tool applicable to various biological experiments, including cell-cycle studies and the classification of environmental bacteria such as cocci and bacilli. In addition, more precise shape-based separation would be possible by more effectively optimizing the microchannel geometries and exploiting the different behaviors of particles according to different morphologies.

ACKNOWLEDGMENTS

This research was supported in part by Grant-in-Aid for Scientific Research A (Grant No. 20241031) from Japan Society for Promotion of Science (JSPS), and for Improvement of Research Environment for Young Researchers from Japan Science and Technology Agency (JST). We thank National Bio-Resource Project (NBRP) of the Ministry of Education, Culture, Sports, Science, and Technology of Japan for kindly providing the budding yeast (Grant No. BY 23849).

[1] R. W. Bauman, in *Microbiology: With Diseases by Body System*, 2nd ed., edited by L. Berriman (Pearson Benjamin Cummings, San Francisco, 2009), Chaps. 4 and 11.
[2] K. H. Schleifer, Syst. Appl. Microbiol. **32**, 533 (2009).
[3] A. Tzur, R. Kafri, V. S. LeBleu, G. Lahav, and M. W. Kirschner, Science **325**, 167 (2009).
[4] P. Fants and R. Brooks, *The Cell Cycle: A Practical Approach* (IRL, Oxford, 1993), Chaps. 1, 2, and 4.
[5] D. Needham, Cell Biophys. **18**, 99 (1991).
[6] N. Pamme, Lab Chip **7**, 1644 (2007).
[7] D. R. Gossett, W. M. Weaver, A. J. Mach, S. C. Hur, H. T. K. Tse, W. Lee, H. Amini, and D. Di Carlo, Anal. Bioanal. Chem. **397**, 3249 (2010).
[8] I. Doh and Y. Cho, Sens. Actuators, A **121**, 59 (2005).
[9] U. Kim, C. Shu, K. Dane, P. Daugherty, J. Wang, and H. Soh, Proc. Natl. Acad. Sci. U.S.A. **104**, 20708 (2007).
[10] A. C. Sabuncu, J. A. Liu, S. J. Beebe, and A. Beskok, Biomicrofluidics **4**, 021101 (2010).
[11] A. Valero, T. Braschler, N. Demierre, and P. Renaud, Biomicrofluidics **4**, 022807 (2010).
[12] K. Zhu, A. S. Kaprelyants, E. G. Salina, M. Schuler, and G. H. Markx, Biomicrofluidics **4**, 022810 (2010).
[13] A. Nilsson, F. Petersson, H. Jönsson, and T. Laurell, Lab Chip **4**, 131 (2004).
[14] F. Petersson, A. Nilsson, C. Holm, H. Jönsson, and T. Laurell, Lab Chip **5**, 20 (2005).
[15] D. Huh, J. H. Bahng, Y. Ling, H. Wei, O. D. Kripfgans, J. B. Fowlkes, J. B. Grotberg, and S. Takayama, Anal. Chem. **79**, 1369 (2007).
[16] N. Pamme and A. Manz, Anal. Chem. **76**, 7250 (2004).
[17] N. Pamme and C. Wilhelm, Lab Chip **6**, 974 (2006).
[18] M. P. MacDonald, G. C. Spalding, and K. Dholakia, Nature (London) **426**, 421 (2003).
[19] M. Yamada and M. Seki, Anal. Chem. **76**, 5465 (2004).
[20] J. Takagi, M. Yamada, M. Yasuda, and M. Seki, Lab Chip **5**, 778 (2005).
[21] M. Yamada and M. Seki, Lab Chip **5**, 1233 (2005).
[22] M. Yamada, K. Kano, Y. Tsuda, J. Kobayashi, M. Yamato, M. Seki, and T. Okano, Biomed. Microdevices **9**, 637 (2007).
[23] S. Migita, K. Funakoshi, D. Tsuya, T. Yamazaki, A. Taniguchi, Y. Sugimoto, N. Hanagata, and T. Ikoma, Anal. Methods **2**, 657 (2010).
[24] M. Matsuda, M. Yamada, and M. Seki, Electron. Commun. Jpn. **94**, 1 (2011).
[25] S. Yang, A. Ündar, and J. D. Zahn, Lab Chip **6**, 871 (2006).
[26] M. Kersaudy-Kerhoas, R. Dhariwal, M. P. Y. Desmulliez, and L. Jouvet, Microfluid. Nanofluid. **8**, 105 (2010).
[27] L. R. Huang, E. C. Cox, R. H. Austin, and J. C. Strum, Science **304**, 987 (2004).

[28] D. W. Inglis, N. Herman, and G. Vesey, Biomicrofluidics **4**, 024109 (2010).
[29] D. Di Carlo, D. Irimia, R. G. Tompkins, and M. Toner, Proc. Natl. Acad. Sci. U.S.A. **104**, 18892 (2007).
[30] Z. Wu, B. Willing, J. Bjerketorp, J. K. Jansson, and K. Hjort, Lab Chip **9**, 1193 (2009).
[31] H. A. Nieuwstadt, R. Seda, D. S. Li, J. B. Fowlkes, and J. L. Bull, Biomed. Microdevices **13**, 97 (2011).
[32] S. Ookawara, R. Higuchi, D. Street, and K. Ogawa, Chem. Eng. J. **101**, 171 (2004).
[33] A. A. S. Bhagat, S. S. Kuntaegowdanahalli, and I. Papautsky, Lab Chip **8**, 1906 (2008).
[34] S. Choi and J. Park, Lab Chip **7**, 890 (2007).
[35] S. Choi, S. Song, C. Choi, and J. Park, Anal. Chem. **81**, 1964 (2009).
[36] H. W. Hou, A. A. S. Bhagat, A. G. L. Chong, P. Mao, K. S. W. Tan, J. Han, and C. T. Lim, Lab Chip **10**, 2605 (2010).
[37] J. P. Beech and J. O. Tegenfeldt, Proceedings of 13th International Conference on Miniaturized Systems for Chemistry and Life Sciences, 2009, p. 800.
[38] J. P. Beech, S. Holm, M. P. Barrett, and J. O. Tegenfeldt, Proceedings of 14th International Conference on Miniaturized Systems for Chemistry and Life Sciences, 2010, p. 1343.
[39] A. Day, C. Schneider, and B. L. Schneider, Methods Mol. Biol. **241**, 55 (2004).
[40] C. J. Behrend, J. N. Anker, and R. Kopelman, Appl. Phys. Lett. **84**, 154 (2004).
[41] D. C. Duffy, J. C. McDonald, O. J. A. Schueller, and G. M. Whitesides, Anal. Chem. **70**, 4974 (1998).
[42] J. C. McDonald, D. C. Duffy, J. R. Anderson, D. T. Chiu, H. Wu, O. J. A. Schueller, and G. M. Whitesides, Electrophoresis **21**, 27 (2000).
[43] See supplementary material at http://dx.doi.org/10.1063/1.3580757 for the detail structures of microdevices A and B, and the behavior of nonspherical triplet particles.
[44] D. Dendukuri, D. C. Pregibon, J. Collins, T. A. Hatton, and P. S. Doyle, Nature Mater. **5**, 365 (2006).
[45] R. F. Shepherd, J. C. Conrad, S. K. Rhodes, D. R. Link, M. Marquez, D. A. Weitz, and J. A. Lewis, Langmuir **22**, 8618 (2006).
[46] D. C. Pregibon, M. Toner, and P. S. Doyle, Science **315**, 1393 (2007).
[47] J. Kim, R. J. Larsen, and D. A. Weitz, J. Am. Chem. Soc. **128**, 14374 (2006).
[48] A. R. Studart, H. C. Shum, and D. A. Weitz, J. Phys. Chem. B **113**, 3914 (2009).
[49] K. Madden, C. Costigan, and M. Snyder, Trends Cell Biol. **2**, 22 (1992).
[50] M. Winey and E. T. O'Toole, Nat. Cell Biol. **3**, E23 (2001).
[51] T. L. Saito, M. Ohtani, H. Sawai, F. Sano, A. Saka, D. Watanabe, M. Yukawa, Y. Ohya, and S. Morishita, Nucleic Acids Res. **32**, D319 (2004).